NJC

Facile strategy for the synthesis of non–covalently bonded and para toluene sulfonic acid functionalized fibrous polyaniline@graphene-PVC nanocomposite for the removal of Congo red

Journal:	*New Journal of Chemistry*
Manuscript ID:	NJ-ART-06-2015-001443.R1
Article Type:	Paper
Date Submitted by the Author:	22-Jun-2015
Complete List of Authors:	Ansari, Mohd; Yeungnam University, South Korea; Yeungnam University, Chemical Engineering Kumar, Rajeev; King Abdulaziz university, Environmental Science Parveen, Nazish; Yeungnam University, School of Chemical Engineering Barakat, M; King Abdulaziz university, Environmental Science; CMRDI, Cho, Moo Hwan; Yeungnam University, Chemical Engineering

Journal Name

ARTICLE

Facile strategy for the synthesis of non-covalently bonded and para toluene sulfonic acid functionalized fibrous polyaniline@graphene-PVC nanocomposite for the removal of Congo red[†]

Mohd Omaish Ansari,[a] Rajeev Kumar,[b*] Nazish Parveen,[a] Mohamed A. Barakat,[b] and Moo Hwan Cho[a*]

This paper reports a simple route for the generation of fibrous polyvinyl chloride (PVC) and graphene (GN) fibers (GN-PVC). The prepared fibrous GN-PVC was functionalized further with para toluene sulfonic acid (*p*TSA) and polyaniline (Pani) to give *p*TSA-Pani@GN-PVC fibers with high functionality. The resulting fibers were characterized by scanning electron microscopy, transmission electron microscopy, Fourier transform infrared spectroscopy, UV-vis diffuse absorbance spectroscopy, X-ray photoelectron spectroscopy, Raman, and X-ray diffraction. The synthesized fibers were used for the adsorption of Congo red (CR) dye from aqueous solutions at different solution pH, initial dye concentrations and temperatures. The Langmuir, Freundlich and Temkin isotherm models were applied to determine the interaction between the synthesized fibers and CR. The adsorption efficacy of the *p*TSA-Pani@GN-PVC composite fiber for the removal of CR was 4.43 and 2.51 times higher than that of PVC and GN-PVC fibers, respectively. Thermodynamic studies showed that the adsorption of CR onto all fibers was exothermic in nature and the spontaneity decreased with increasing solution temperature.

Introduction

The increasing industrialization worldwide has resulted in an increase in the formation of wastewater, which demands newer and more efficient processes for their treatment before being discharged into the natural environment. Synthetic complex organic dyes as coloring materials are used widely in textile industries, and the wastewater from them contains a large amount of dyes.[1] The removal of dyes from wastewater has attracted considerable attention due to the toxic nature of most dyes. Most synthetic dyes are resistant to natural degradation, and have allergic, carcinogenic and mutagenic properties; hence, they pose a health hazard to living beings. Diseases, such as dysfunction of the kidneys, failure of the reproductive system, liver, brain, and central nervous system have also been reported.[2] Even in very small quantities, dyes can be very toxic and may lead to changes in salinity and visible coloration of water, reducing sunlight penetration and hindering the photosynthesis process.[3] Therefore, the decolorization of dyes is another important aspect of wastewater treatment before being discharged into the environment.

Many physical and chemical methods, such as adsorption, coagulation, precipitation, and filtration have been used to remove the harmful dyes from colored wastewaters.[4] Among them, adsorption is the most economical and effective method for the removal of dyes because of the low cost, easy access and effective dye removal because the dissolved dye compounds attach themselves to the surface of the adsorbents.[5] The adsorbents can be synthesized easily with different functionalities that might allow selective adsorption for practical applications. On the other hand, most powdered adsorbents do not process selectivity and is difficult to recover them from aqueous solution because of their small size. Therefore, the development of surface charged adsorbent materials with specific selectivity from aquatic media are needed.

The wide variations in functionality, surface area, porosity, and the ease of separation has made the use of polymeric materials an alternative to activated carbon for the removal of specific pollutants from contaminated water.[6] Recently, polyaniline (Pani) has been used as an adsorbent for adsorption of proteins,[7] DNA,[8] heavy metals,[9] and dyes.[10] Pani can be prepared in different forms depending on the synthesis route, such as acidic or basic treatments. In acid media, Pani chains become protonated or oxidized and

acquire positive charges localized over the polymeric backbone.[11] The positive charges are counter balanced by anions that are adsorbed by the Pani chains. Pani can be discharged (neutral) by treating the polymer with bases, and consequently changes its electrical properties from a metallic to insulating state. Considering the charge-discharge phenomenon induced by the acid-base treatments, an electrostatic interaction between the charged Pani and ionic species can be assumed. Therefore, Pani may be an exciting candidate for the selective adsorption of ionic specie.

Organic polymers, such as polyvinyl chloride (PVC), have emerged as suitable replacements for inorganic and other materials owing to their high pollutant removal capacity and adjustable surface chemistry. PVC can be used as a suitable template for the synthesis of composite materials with the desired functionality for the removal of dye pollutants. In a previous report, conducting Pani was coated on CNT and used as an adsorbent because of its electrical conductivity and electronegativity.[12] In addition, they have an advantages of less sludge generation and are effective in both batch and column mode systems.

In this study, anionic dye selective Pani and para toluene sulfonic acid (pTSA) functionalized fibrous pTSA-Pani@GN-PVC composite were prepared using a simple deposition technique. The fibrous morphology is expected to increase the surface area resulting in high adsorption properties. The adsorption performance of pTSA-Pani@GN-PVC for the removal of Congo red (CR) dye from aqueous solutions was evaluated. The role of the solution pH, temperature and CR dye concentration on the adsorption of CR onto pTSA-Pani@GN-PVC was also investigated.

Experimental

Materials

Aniline and para toluene sulfonic acid (pTSA) were acquired from Sigma Aldrich, whereas potassium persulphate (PPs), tetrahydrofuran (THF), hydrochloric acid, ammonia solution (35%), and methyl alcohol were purchased from Duksan Pure Chemicals Co. Ltd., South Korea. GN was purchased from Iljin Nano Tech, Seoul, Korea (thickness 8 nm and average length 500 nm). PVC (average molecular weight 1020) was obtained from Yakuri Pure Chemicals, Japan. Congo red (CR); $C_{32}H_{22}N_6Na_2O_6S_2$, MW: 696.66 g/mol was acquired from Techno Pharmachem Haryana, India. The water used in these experiments was de-ionized water obtained from a PURE ROUP 30 water purification system.

Methods

The microstructures of the PVC, GN-PVC and pTSA-Pani@GN-PVC were examined by scanning electron microscopy (SEM, HITACHI-S4800) and field emission transmission electron microscopy (FE-TEM, Tecnai G2 F20, FEI, USA) at an accelerating voltage of 200kV. Phase analysis was performed by X-ray diffraction (XRD, PANalytical, X'pert PRO-MPD, Netherland) using Cu Kα radiation (λ = 0.15405 nm). The functional groups and their interactions were examined by Fourier transform infrared

(FTIR, Excalibur series FTS 3000 Bio-Rad spectrometer) spectroscopy. The UV-visible diffuse absorbance spectra were measured using ultraviolet-visible-near infrared spectrophotometer (UV-VIS-NIR, Cary 5000, VARIAN, USA). The chemical state and surface composition were analyzed by X-ray photoelectron spectroscopy (XPS, ESCALAB 250 XPS system, Thermo Fisher Scientific U.K.) using a monochromatized l Kα x-ray source (hν = 1486.6 eV).

Synthesis of the PVC, GN-PVC and pTSA-Pani@GN-PVC nanocomposite fibers

The Pani and pTSA functionalized Pani@GN-PVC fibers were prepared in three steps. The first step involved the synthesis of the GN-PVC nanocomposite by mixing GN in the THF solution of PVC, followed by a deposition technique to prepare the GN-PVC fibers and subsequent functionalization with Pani and pTSA. In a typical process, PVC (2g) was first dissolved in 50 mL of THF with continuous stirring for 24 h for complete dissolution. GN (5% wt. of PVC) was mixed with the above solution with continuous stirring and occasional shaking in a bath ultrasonic system for 5 min to allow the proper dispersion of GN inside the THF solution of PVC. Subsequently, the mixture was poured into distilled water with vigorous stirring to obtain the GN-PVC fibers.

The obtained GN-PVC fibers were further functionalized with Pani under dilute polymerization condition. In a typical process, 1 g of GN-PVC fibers was added to 500 mL of 1M HCl followed by agitation in an ultrasonic bath for proper dispersion, which was followed by the addition of 0.25 mL of the aniline monomer. The entire system was stirred vigorously and a solution of the oxidant (0.5 M PPs in 500 mL 1M HCl) was added drop wise to the above dispersion of GN-PVC fibers and aniline to initiate the polymerization reaction. The reaction mixture was stirred constantly for 12 hours, after which the solution was filtered. Thus prepared Pani@GN-PVC slurry after filtration was washed with an excess of water and methanol to remove the residual PPs and Pani oligomers. The nanocomposite fibers was de-doped in a 1M ammonia solution and then washed with water and methanol. The prepared emeraldine base of the Pani@GN-PVC nanocomposite (1g) fibers was doped with 100 mL of a 1M pTSA solution for 12 hours followed by filtration under vacuum suction to give the pTSA functionalized pTSA-Pani@GN-PVC fibers.

Adsorption studies

The adsorption of CR dye onto the synthesized fibers was studied in a batch process by adding 0.02 g fiber to 20 mL of the dye solution at fixed concentration, pH and temperature. To determine the effect of the solution pH, a series of conical flasks were prepared containing 20 mL of 20 mg/L dye solution and pH ranging from 4.5 to 9.5. The pH of the dye solution was adjusted using 0.1 M HCl and 0.1M NaOH. Subsequently, 0.02 g of fibers were added to each flask and placed into water bath shaker at 200 rpm. The dye adsorption equilibrium studies were performed by varying the initial dye concentration from 10 to 50 mg/L at pH 4.5 and 30 ℃. The thermodynamic studies were performed by taking 20 mL of a 20

mg/L dye solution and 0.02 g fibers at 30, 40 and 50 °C under shaking conditions at 200 rpm. After reaching equilibrium, the amount of CR remaining in the solution was determined using a HACH LANGE DR 6000 UV-visible spectrophotometer at 495 nm. The adsorption capacity of the fibers for CR was calculated using the following equation:

$$q_e = (C_0 - Ce)V/m \qquad (1)$$

where q_e is the amount of CR adsorbed per unit mass of fiber (mg g^{-1}), C_0 and Ce is the initial and equilibrium CR concentration (mg L^{-1}), respectively. V is the volume of CR solution (L) and m is the mass of fiber (g).

Results and discussion

Proposed mechanism for the synthesis of the *p*TSA-Pani@GN-PVC nanocomposite fibers

The *p*TSA-Pani@GN-PVC nanocomposite fibers were prepared by the surface functionalization of GN-PVC fibers by Pani, followed by doping with *p*TSA to impart additional functionality. The immiscible solvent system of THF and water was used to prepare the PVC and GN-PVC fibers. The dispersed GN and PVC in THF under vigorous stirring precipitated readily in water owing to its insolubility in water. The digital photograph revealed highly dispersed fibers of PVC, GN-PVC and *p*TSA-Pani@GN-PVC (Fig. 1a). The SEM image showed highly fibrous morphology of the PVC fibers (Fig. 1b), which is expected to possess high surface area and may provide an ideal template for further functionalization. The *p*TSA-Pani@GN-PVC fibers also showed similar long strands varying upto several micrometers in length as evident from Fig 1c and 1d. The functionality of the fibers is expected to increase after the incorporation of GN into the PVC matrix. Dilute polymerization of aniline and further doping of *p*TSA on the GN-PVC fibers imparted additional functionality, which may be beneficial for the selective adsorption of dyes.
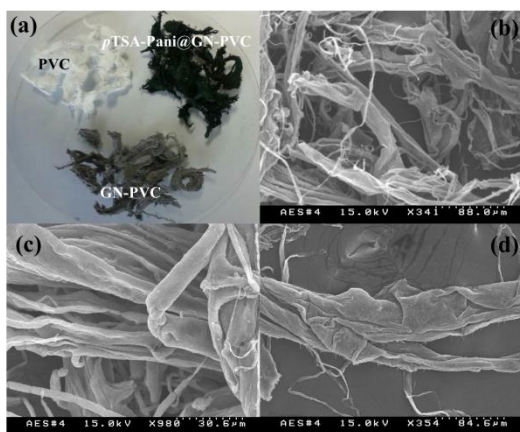
Fig. 1. Digital photograph of (a) PVC, GN-PVC and *p*TSA-Pani@GN-PVC fibers; (b) SEM image of the PVC fibers and (c),(d) SEM image of *p*TSA-Pani@GN-PVC fibers

Morphological and Surface area analysis

TEM was performed for detailed morphological studies of *p*TSA-Pani@GN-PVC fibers (Fig. 2a, b). Long interconnected fibrous structures with different thicknesses could be seen throughout with GN nanosheets well dispersed in the system. The fibers grew up to several micrometers in length and a single fiber can be seen composed of many small thin fibers interconnected together. The aniline monomers polymerized on the surface were not clearly visible because of the very dilute polymerization conditions. The HR-TEM image (Fig. 2d) showed the lattice fringes of GN inside PVC with a spacing of 0.32 nm, which is in good agreement with the reported literature.[13] However, not clearly distinct lattice fringes of GN may be due to the non-conducting nature of PVC and its surface covering with Pani and *p*TSA. The surface area of the PVC, GN-PVC and *p*TSA-Pani@GN-PVC were found to be 0.8881, 0.6403 and 0.0894 m^2/g, respectively.
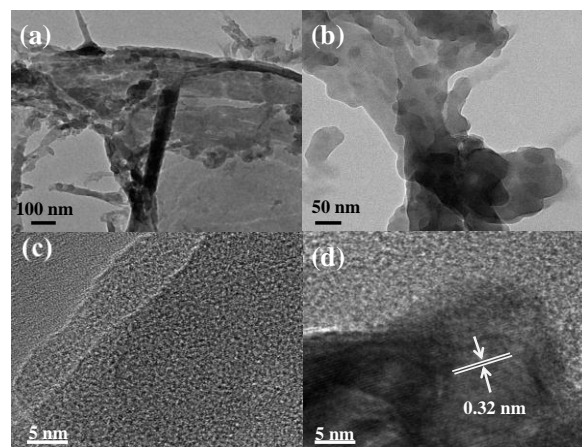
Fig. 2. TEM (a,b) and HR-TEM (c,d) image of the *p*TSA-Pani@GN-PVC fibers.

Compositional Study

XPS measurements were conducted for the composition and surface analysis of fibers (Fig. 3). It revealed that the surface of PVC consist of mainly C1s and Cl 2p with 76 and 23 % atomic ratios. For PVC, the features in C 1s fitted core-line show the peak positions at 284.6 and 286.4 eV due to the -CH_2- and C-O-H groups, respectively. In Cl 2p spectra two characteristic peaks of Cl $2p_{3/2}$ and Cl $2p_{1/2}$ were observed at 200.3 and 198.4 eV, respectively which confirmed the existence of a C–Cl bond[14]. In the case of *p*TSA-Pani@GN-PVC, it consisted of mainly C and O (71 and 15%) with small amounts of N, S and Cl (6,4 and 2%) peaks. To determine the chemical components and the oxidation states of each element (N, Cl, O, S and C), high-resolution XPS spectra of N1s, Cl 2p, O 1s, S 2p and C 1s were analysed. The observance of C 1s peak with binding energy of 285 eV and broad peak for Cl 2p at 201 eV confirmed the existence of a C–Cl bond. The slight change in the mixing and binding energy around 200.4 and 202.2 eV of two bands of C1s in the case of *p*TSA-Pani@GN-PVC nanocomposite fiber is probably due to strong interaction between the carbon of GN and chlorine of PVC. The N 1s peak at 399.7 and 401.9 eV

corresponds to the positively quinoid amine and benzenoid amine groups hence confirming the presence of Pani[15,16]. The peak arising at 168.05 and 169.4 eV in the S 2p spectrum is due to the presence of -SO$_3$ group of pTSA[17].
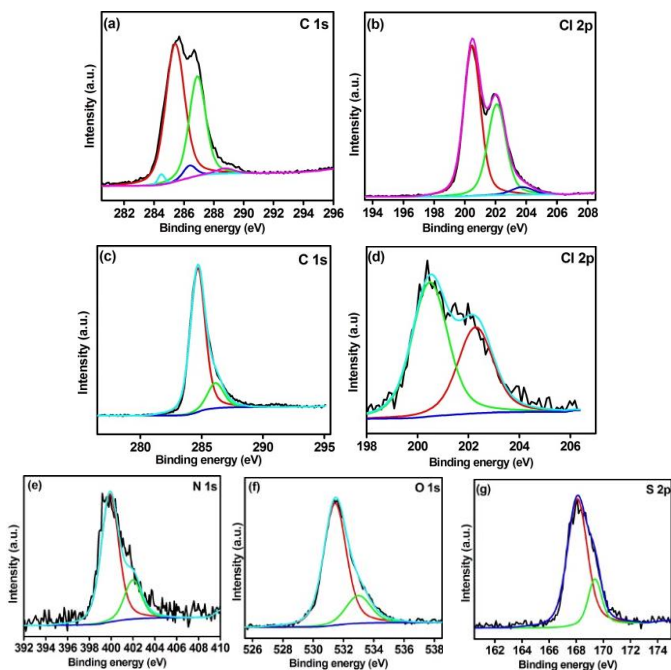
Fig. 3. (**a**) C 1s core level spectra, (**b**) Cl 2p core level spectra of PVC and (**c**) C 1s core level spectra, (**d**) Cl 2p core level spectra, (**e**) N 1s core level spectra, (**f**) O 1s core level spectra, and (**g**) S 2p core level spectra of pTSA-Pani@GN-PVC.

Structural Analysis
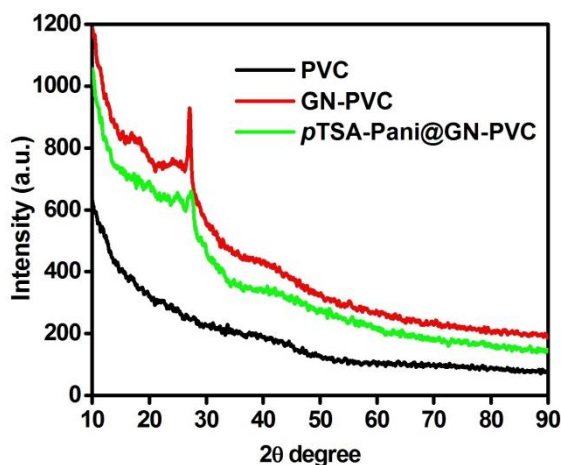
Fig. 4. XRD pattern of PVC, GN-PVC and pTSA-Pani@GN-PVC fibers.

Fig. 4 shows the XRD patterns of PVC, GN-PVC and pTSA-Pani@GN-PVC fibers. Pure PVC did not show any XRD peaks from 10 to 80° 2θ because of its highly amorphous nature[18]. In the case of GN-PVC and pTSA-Pani@GN-PVC fibers, the diffraction peaks were due mainly to GN. A single large diffraction peak at 26.53° 2θ,

which is very close to the diffraction of the (002) crystalline plane of a graphite sheet indicates the presence of GN.[19,20] The observance of a broad peak of GN and the absence of peaks of GN at higher 2θ values of 45.29°, 44.58° and 54.47 suggests that the amorphous PVC has a significant effect on the crystallinity of GN and there is an effective interaction of GN with PVC, which may lead to better translation of the properties of GN and PVC into a single GN-PVC system. The peak for Pani in pTSA-Pani@GN-PVC was strongly suppressed due to the dilute polymerizations conditions and large amount of GN.

Raman analysis
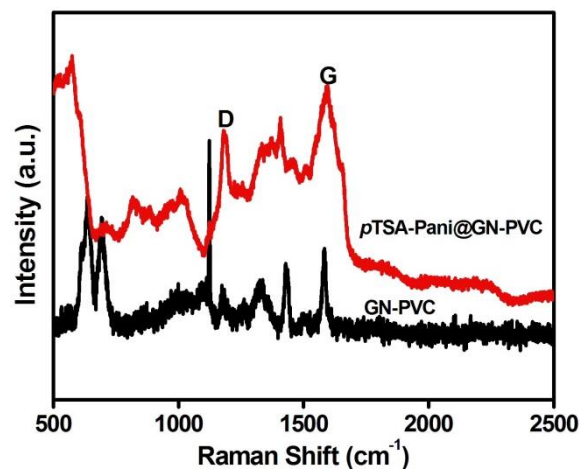
Fig. 5. Raman spectra of GN-PVC and pTSA-Pani@GN-PVC fibers.

Raman spectroscopy is a powerful tool for determining the microstructure of carbon based materials[21]. The Raman spectra of the GN-PVC fibers nanocomposite showed two characteristic bands, the D band and G band (Fig. 5). The D band was attributed to a disordered in the graphite structure, whereas the G band showed the structural intensity of the sp^2 hybridized carbon atoms[22]. The other bands in the range of ~600-700 cm^{-1} are associated with (C-Cl) stretching while the bands at ~1100 and 1450 cm^{-1} are due to the ~(C-C) and (C=C) stretching vibrations respectively. The presence of D and G bands in the Raman spectra of the GN-PVC fibers nanocomposite suggests that the nanocomposite contains both sp^3 and sp^2-hybridized carbon atoms. The difference in the band intensity ratio (ID/IG) of the GN-PVC and pTSA-Pani@GN-PVC nanocomposite can be used to estimate the relative degree of defects in the GN. The value of intensity ratio of the D and G bands (ID/IG) was calculated to be 1.20 and 0.79 for GN-PVC and pTSA-Pani@GN-PVC fibers respectively. The increase in the ID/IG ratio of fibers nanocomposite obtained in our case in comparison to GN indicates an increase in the defects in the lattice of GN[23]. The positions of the D and G bands were also shifted, confirming that defect was formed due to the Pani coating and doping of pTSA in the pTSA-Pani@GN-PVC fibers.

Functional group and interactional analysis

Fig. 6 shows the FTIR spectra of PVC, GN-PVC and *p*TSA-Pani@GN-PVC fibers. Pure PVC shows all the vibrational modes, which is consistent with the report of Ramesh et al.[24] The band at ~2971 and 2900 cm^{-1} we assigned to the C–H stretching vibration modes and presence of methylene ($-CH_2-$) group, whereas the other bands at ~1255 and ~959 cm^{-1} are due to the C–H rocking mode and trans C–H wagging mode, respectively. The vibration due to the C–Cl stretching mode was observed at 834 cm^{-1}, whereas the band at 686 cm^{-1} was assigned to the C–H wagging mode. GN-PVC shows all the peaks corresponding to PVC with a slight blue shift and reduced intensity. This might be due to the surface interaction of GN with the double bonds of PVC via a π-π interaction. In the case of *p*TSA-Pani@GN-PVC fibers, there was a further decrease in intensity, which confirmed the surface functionalization by Pani. The characteristic N–H stretching vibration mode of Pani was not distinct due to the dilute polymerization conditions. The peaks at 1569, 805, 1245, 1132, and 1030 cm^{-1} corresponds to the vibration modes of *p*TSA, confirming the successful functionalization of GN-PVC fibers by Pani and *p*TSA.[25] After the adsorption of CR on the PVC, GN-PVC and *p*TSA-Pani@GN-PVC fibers, a significant change in the intensity or shift in the position of the peaks for imine, amine, benzonoid, quionoid groups occurs, due to the strong interaction between CR, Pani and GN (π-π and electrostatic interaction) indicating that these groups were the major contributors for the interaction of CR onto the fiber surface. [26,27]

higher absorption by GN. The surface coating of Pani over the *p*TSA-Pani@GN-PVC fibers suppressed the peaks attributed to the PVC or GN-PVC absorption regions due to the dominance of much higher absorption by Pani in both the UV and visible regions.[28] This also shows the successful functionalization of GN-PVC fibers by Pani, which might be beneficial for the adsorption studies.
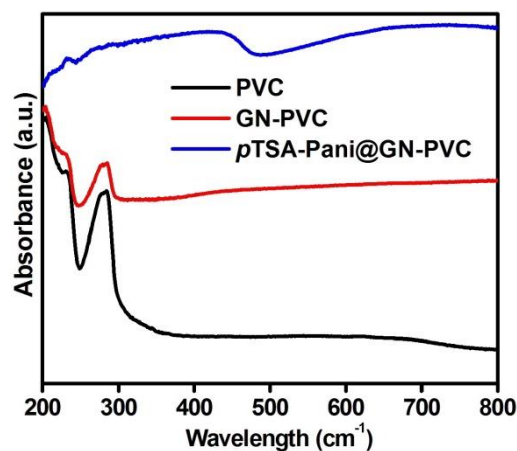
Fig. 7. UV-vis diffuse absorbance of PVC, GN-PVC and *p*TSA-Pani@GN-PVC fibers.

Effect of solution pH and adsorption mechanism
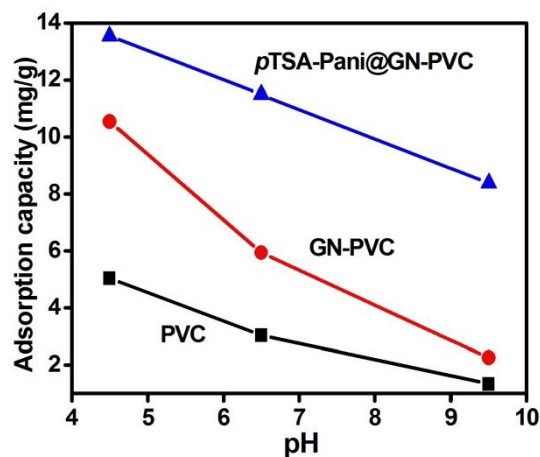
Fig. 8. Effect of the solution pH on CR adsorption onto the PVC, GN-PVC and *p*TSA-Pani@GN-PVC fibers (T: 30 ℃, m: 0.025g, V: 20 ml, time: 6h Conc.: 20mg/L).

Fig. 6. FTIR of PVC, GN-PVC and *p*TSA-Pani@GN-PVC fibers before and after adsorption of CR.

Optical Analysis

A UV-vis diffuse absorbance study was conducted to further confirm the surface functionalization by Pani (Fig. 7). The absorbance spectra of PVC and GN-PVC showed three absorbance peaks at λ = 207, 231 and 281 nm, which were assigned to the n–σ*, n–π* and π–π* transitions, respectively. Compared to PVC, the GN-PVC fibers showed an increase in absorption intensity due to the

The effects of the initial solution pH was examined in the pH ranges from 4.5-9.5 because, under highly acidic conditions, CR tends to change color from red to blue due to ammonium-azonium tautomerism within the dye molecule.[29,30] Fig. 8 shows the effects of the solution pH. The results suggest that the adsorption capacity of the fibers for CR depends strongly on the solution pH and the maximum removal of CR was observed at pH 4.5. The trend for CR removal was observed as PVC<GN-PVC<*p*TSA-Pani@GN-PVC, showing that the adsorption capacity increased with increasing functionality of the fiber. This adsorption behavior of CR onto the fibers can be explained based on the functionality of the fibers and

surface charge of the dye. PVC showed the lowest adsorption because it does not have any specific functional group for CR binding, whereas GN-PVC showed good adsorption compared to PVC, which might be due to the π–π interaction between GN and CR. The higher adsorption capacity of *p*TSA-Pani@GN-PVC was attributed mainly to the electrostatic interaction between the negatively charged sulfonate groups of CR and the positively charged amine group of Pani at acidic pH. As the solution pH increased, deprotonation of Pani took place and the number of negatively charge sites increased, which decreased the adsorption of CR by electrostatic repulsion.[31] On the other hand, at higher pH, the limited adsorption of CR was observed, which may be due to the combination of other sorption forces, such as van der Waal, hydrogen bonding between the nitrogen and oxygen atom containing functional groups of adsorbent and adsorbate, and π−π interactions between the aromatic ring of GN and CR molecules.[31] The surface area of a material plays vital role in adsorption process and the adsorbent with higher surface area generally shows larger adsorption capacity.

PVC fibers shows higher surface area (0.8881 m^2/g) than GN-PVC (0.6403 m^2/g) and *p*TSA-Pani@GN-PVC (0.0894 m^2/g), revealing that the higher surface area is not the main factor in the enhanced adsorption of CR onto *p*TSA-Pani@GN-PVC. The BET result indicates that as the functionality of the fibers increased the surface area decreased. This may be due to decease in the diffusion of the gas molecules into the pores, hindered by the GN, *p*TSA and Pani. Similar adsorption behaviours have been reported for the modified adsorbent by other researchers also.[32,33]

Fig. 9 presents a schematic diagram of the possible interaction between CR and *p*TSA-Pani@GN-PVC.
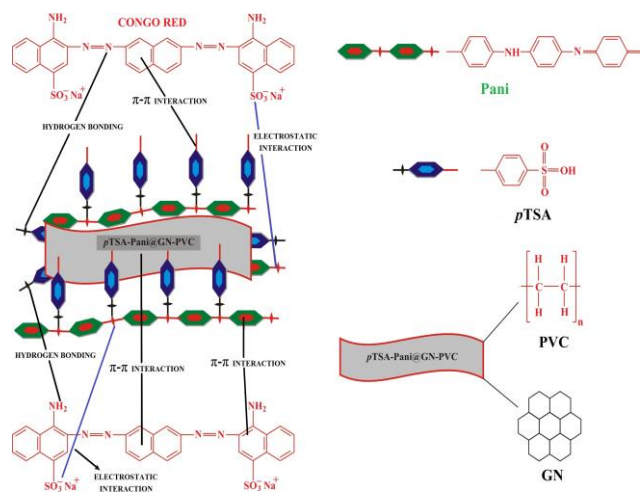
Fig. 9. Schematic diagram of the possible interactions between CR and *p*TSA-Pani@GN-PVC fiber.

Adsorption isotherm studies

The dye uptake capacities of the all three fibers were studied in the range of concentrations from 10 to 50 mg/L, as shown in Fig. 10. The removal of CR increases with increasing initial concentration of CR molecules in the solution. This behavior can be explained based on the higher concentration gradient of dye molecules in solution, which produce the higher driving force by the pressure gradient (ΔC = $C_0−C_e$); hence, facilitating better adsorption.[34] For a better understating of the distribution of CR molecules between the solution and solid phase, the Langmuir, Freundlich and Temkin isotherm models were used to fit the adsorption equilibrium data. The Langmuir isotherm model is valid for monolayer adsorption onto the adsorbent surface, which contains a finite number of identical active sites and no transmigration of the adsorbate in the plane of the surface.[35] The linear equation for the Langmuir isotherm is as follows:

$$\frac{1}{q_e} = \frac{1}{q_m b \, C_e} + \frac{1}{q_m} \qquad (2)$$

where q_e (mg/g) is the amount of CR molecules adsorbed at equilibrium, C_e (mg/L) is the equilibrium concentration of CR, q_m (mg/g) is the maximum monolayer adsorption capacity, and b (L/mg) is the adsorption equilibrium constant. The values of the Langmuir isotherm constants were calculated from a plot of $1/q_e$ vs. $1/C_e$ (Fig. not shown).

The Freundlich isotherm model assumes that the adsorption of adsorbate species occurs through a multilayer and energetically heterogeneous system, which is characterized by the heterogeneity factor, $1/n$.[36] The linear equation for the Freundlich isotherm is as follows:

$$\ln q_e = \ln K_F + \frac{1}{n} \ln C_e \qquad (3)$$

where K_F and n are the Freundlich constants, which indicate the adsorption capacity and adsorption intensity. The values of the Freundlich isotherm parameters were calculated from a plot of ln q_e vs. ln C_e (Fig. not shown).

The Temkin isotherm model is based on the adsorbent-adsorbate interactions and along with the saturation of adsorbent active sites, the adsorption energy decreases linearly than decreasing exponentially.[37] The linear equation for Temkin isotherm model is as follows:

$$Q_e = B \ln A + B \ln C_e \qquad (4)$$

where A and B are the Temkin isotherm parameters, which are related to the equilibrium binding constant (L/mg) and the heat of adsorption (kJ/mol), respectively. The values of the Temkin constants were calculated from a plot of q_e vs. ln C_e (Fig. not shown).

Table S1 lists the values of adsorption isotherm parameters calculated from their respective plots. From the calculated adsorption isotherm parameters, the Langmuir and Temkin isotherm models showed the highest agreement with the adsorption data for CR removal. Both the Langmuir and Temkin models show better correlation coefficients than the Freundlich isotherm model.[38,39] These results indicates that monolayer adsorption has occurred through the finite number of identical and equivalent sites. The correlation coefficient (R^2) values for Temkin model is fairly close to the Langmuir model (R^2) which revealed a uniform distribution of binding energies over all the binding sites on the fibers surface, supporting the monolayer adsorption mechanism. The maximum

monolayer adsorption capacity of PVC, GN-PVC and *p*TSA-Pani@GN-PVC were 10.75, 27.027 and 45.454 mg/g, respectively.
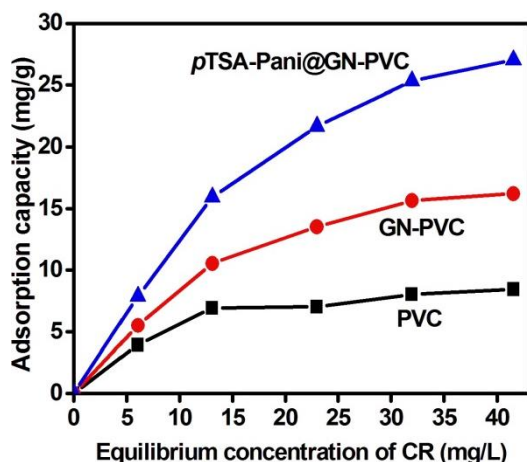
Fig. 10. CR adsorption isotherms onto the PVC, GN-PVC and *p*TSA-Pani@GN-PVC fibers (pH: 4.5, T: 30 ℃, m: 0.025g, V: 20 ml, time: 6h).

Thermodynamic studies

The effect of temperature on the adsorption behavior of CR onto all three fibers was performed at 30, 40 and 50 ℃. The adsorption capacity of all fibers decreased with increasing solution temperature from 30 to 50 ℃. The adsorption capacity of the PVC, GN-PVC and *p*TSA-Pani@GN-PVC fibers at 30 ℃ were 6.92, 10.54 and 15.95 mg/g, respectively, which decreased to 1.66, 7.05 and 10.28 mg/g, respectively. These results suggest that the adsorption of CR onto the PVC based fibers was exothermic in nature, and a low temperature condition is more favorable for the adsorption process. For a better understanding of the CR adsorption process, the free energy change ($\Delta G°$, kJ/mol) was calculated from the Gibbs equations:

$$\Delta G° = -RT \ln K_c \qquad (5)$$

$$K_c = \frac{C_{AE}}{C_{SE}} \qquad (6)$$

where K_c is the adsorption equilibrium constant and R is the gas constant (8.314 J mol^{-1} K^{-1}), respectively, T is the temperature (K). C_{AE} and C_{SE} (mg/L) are the amount of dye adsorbed and dye remaining in solution at equilibrium, respectively. Table S2 lists the free energy change for the CR adsorption calculated from the Gibbs equation. The values of $\Delta G°$ showed that the adsorption of CR onto PVC was non-spontaneous at all temperatures studied, whereas for the GN-PVC fibers, it showed spontaneous behavior, which becomes non-spontaneous with increasing solution temperature. On the other hand, the adsorption of CR onto *p*TSA-Pani@GN-PVC nanofibers was spontaneous. These anomalous behaviors can be explained based on the change in the adsorption capacity of all the studied fibers. PVC showed poor adsorption and after equilibrium, the C_{AE} to C_{SE} ratio become low, which causes unfavorable and non-spontaneous adsorption.

Moreover, the enthalpy change ($\Delta H°$) and entropy change ($\Delta S°$) were calculated from the Van't Hoff equation.

$$\ln K_c = \frac{\Delta S^0}{R} - \frac{\Delta H^0}{RT} \qquad (7)$$

The values of $\Delta H°$ and $\Delta S°$ were calculated from Van't Hoff plot, as shown in Fig. 11 and are mentioned in Table S2. The values of $\Delta H°$ were negative for the PVC, GN-PVC and *p*TSA-Pani@GN-PVC fibers, suggesting that the adsorption of CR onto all studied fibers was exothermic in nature. Furthermore, the values of $\Delta S°$ were also negative, highlighting the increase in randomness at the solid solution interface. From the thermodynamic study, it can be concluded that adsorption of CR was more favorable at low temperatures.
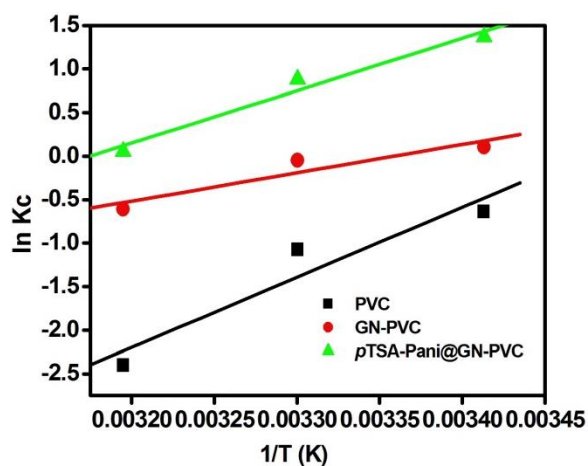
Fig. 11 Van't Hoff Plot for the adsorptive removal of CR onto PVC, GN-PVC and *p*TSA-Pani@GN-PVC fibers.

Conclusions

In this study, PVC, GN-PVC and *p*TSA-Pani@GN-PVC, fibers were synthesized using a facile strategy for the removal of CR dye from an aqueous solution. The adsorption capacity of the synthesized fibers for CR was observed in the following order: *p*TSA-Pani@GN-PVC>GN-PVC>PVC. An acidic solution pH favors the removal of CR and the highest adsorption was obtained at pH 4.5. The Langmuir isotherm model was best fitted to the adsorption equilibrium data, indicating the monolayer adsorption of CR onto all studied fibers with the maximum monolayer adsorption capacity of 10.75, 27.027 and 45.454 mg/g onto PVC, GN-PVC and *p*TSA-Pani@GN-PVC, respectively. Several forces, such as hydrogen bonding, $\pi-\pi$ skating, electrostatic interaction, and van der Wall's forces, were expected to be responsible mainly for the removal of CR by the functionalized *p*TSA-Pani@GN-PVC fibers. The simple and ease of synthesis, and relatively high adsorption capacity nature indicate that the *p*TSA-Pani@GN-PVC fibers can be used effectively for the treatment of reactive dye effluents.

Acknowledgements

Notes and references

aSchool of Chemical Engineering, Yeungnam University, Gyeongsan-si, Gyeongbuk 712-749, South Korea. Phone: +82-53-810-2517; Fax: +82-53-810-4631.

bDepartment of Environmental Sciences, Faculty of Meteorology, Environment and Arid Land Agriculture, King Abdulaziz University, Jeddah 21589, Saudi Arabia.

***Corresponding author Email:** mhcho@ynu.ac.kr; and olifiaraju@gmail.com*

†Electronic Supplementary Information (ESI) available: [Table S1 and Table S2] See DOI: 10.1039/b000000x/

1 R. Bhattacharyya, and S. K. Ray, *Applied Clay Science*, 2014, **101**, 510–520.

2 P. F. Bladin, *J. Clin. Neuroscience*, 2014, **21**, 33–39.

3. M. H. Farzana, S. Meenakshi, *Int. J. Biol. Macromol.*, 2015, **72**, 900–910

4 E. Brillasa, C. A. Martínez-Huitle, *Applied Catalysis, B*; 2009, **87**, 105–145.

5 R. Kumar, M. O. Ansari, M. A. Barakat, *Chem. Eng. J.*, 2013, **228**, 748–755.

6 B. Pan, B. Pan, W. Zhang, L. Lv, Q. Zhang, S. Zheng, *Chem. Eng. J.*, 2009, **151**, 19–29.

7 L. P. Wang, W. Wang, L. Di, Y. N. Lu, J. Y. Wang, *Colloids and Surf., B*, 2010, **80**, 72–78.

8 J. C. Medina-Llamasa, A. E. Chávez-Guajardoa, C. A. S. Andradeb, K. G. B. Alvesc, C. P. de Melo, *J. Colloid Interface Sci.*, 2014, **434**, 167–174.

9 R. S. Norouzian, M. M. Lakouraj, *Synth. Met.*, 2015, **203**, 135–148.

10 M. A. Salem, React. Funct. Polym. 70, 2010, 707–714

11 M. O. Ansari, F. Mohammad, *Sens. Actuators, B*, 2011, **157**, 122–129.

12 R. Kumar, M. O. Ansari, M. A. Barakat, *Ind. Eng. Chem. Res.* 2014, **53**, 7167−7175

13 S. Bhandari, M. Deepa, A. G. Joshi, A. P. Saxena, A. K Srivastava, *Nanoscale Research Letters*, 2011, **6**, 424.

14 B. Balakrishnan, D. S. Kumar, Y. Yoshida, A. Jayakrishnan, *Biomaterials*, 2005, **26**, 3495–3502.

15 S. Bai, Y. Zhao, J. Sun, Y. Tian, R. Luo, D. Li, A. Chen, *Chem. Commun.*, 2015, **51**, 7524-7527.

16 M. Mumtaz, C. Labrugere, E. Cloutet, H. Cramail, *Langmuir* 2009, **25**(23), 13569–13580.

17 H. Gu, S. B. Rapole, J. Sharma, Y. Huang, D.i Cao, H. A. Colorado, Z. Luo, N. Haldolaarachchige, D. P. Young, B. Walters, S. Wei, Z. Guo, *RSC Advances*, 2012, **2**, 11007–11018.

18 C. H. Chen, C. C. Teng, M. S. Tsai, F. S. Yen, *J. Polym. Sci., Part B: Polym. Phys.*, 2006, **44**, 2145–2154.

19 M. O. Ansari, S. K. Yadav, J. W. Cho, F. Mohammad, *Composites Part B*, 2013, **47**, 155-161

20 M. Zhou, J. Tang, Q. Cheng, G. Xu, P. Cui, L. C. Qin, *Chem. Phys. Lett.*, 2013, **572**, 61–65.

21 X. Yan, J. Chen, J. Yang, Q. Xue, P. Miele, *ACS Appl. Mater. Interfaces,* 2010, **2**(9), 2521–2529

22 K. Parvez, Z.S. Wu, R. Li, X. Liu, R. Graf, X. Feng, K. Müllen, J. Am. Chem. Soc,. 2014, **136**, 6083–6091

23 P. Mahanandia, F. Simon, G. Heinrich, K. Kar Nanda, *Chem. Commun*., 2014, 50, 4613–4615

24 S. Ramesh, L. J. Yi, *Ionics*, 2009, **15**, 413–420.

25 R. S. Tipson, *J. Am. Chem. Soc.*, 1952, **74** (5), 1354–1354.

26 S. Goswami, U. N. Maiti, S. Maiti, S. Nandy, M. K. Mitra, K. K. Chattopadhyay, *Carbon*, 2011, **49**, 2245–2252.

27 M. Fang, Z. Chen, S. Wang, H. Lu, *Nanotechnology*, 2012, **23**, 085704.

28 M. O. Ansari, M. M. Khan, S. A. Ansari, K. Raju, J. Lee, M. H. Cho, *ACS Appl. Mater. Interfaces*, 2014, **6**, 8124−8133

29 J. Barkauskas, I. Stankevicien, J. Daksevic, A. Padarauskas, *Carbon*, 2011, **49**, 5373–5381.

30 R. Ahmad, R. Kumar, *Appl. Surf. Sci.*, 2010, **257** (5), 1628-1633

31 V. Janaki, K. Vijayaraghavan, A. K. Ramasamy, K. J. Lee, B. T. Oh, S. Kamala-Kannan, *J. Hazard. Mater.*, 2012, **241–242**, 110–117.

32 W. Teng, Z. Wu, D. Feng, J. Fan , J. Wang, H. Wei, M. Song, D. Zhao, *Environ. Sci. Technol.*, 2013, **47 (15)**, 8633–8641.

33 G. Yang, L. Tang, Y. Cai, G. Zeng, P. Guo, G. Chen, Y. Zhou, J. Tang, J. Chen W. Xiong, *RSC Adv.*, 2014, **4**, 58362–58371.

34 B. H. Hameed, D. K. Mahmoud, A. L. Ahmad, *Colloids Surf. A*, 2008, **316**, 78–84.

35 I. Langmuir, *J. Am. Chem. Soc.*, 1918, **40**, 1361–1403.

36 H. Freundlich, *J. Phys. Chem.*, 1907, 57, 385–470

37 M. I. Temkin, V. Pyzhev, *Acta Physiochem URSS*, 1940, **12**, 217–222

38 Q. Du, J. Sun, Y. Li, X. Yang, X. Wang, Z. Wang, L. Xia, *Chem. Eng. J.*, 2014, **245**, 99–106

39 H. Guo, J. Chen, W. Weng, Z. Zheng, D. Wang, *J. Ind. Eng. Chem. 20*, 2014, 3081–3088.